Journal of Asian Earth Sciences 174 (2019) 205–217

Contents lists available at ScienceDirect

Journal of Asian Earth Sciences

journal homepage: www.elsevier.com/locate/jseaes

Full length article

The burial and exhumation history of the Liuqu Conglomerate in the Yarlung Zangbo suture zone, southern Tibet: Insights from clumped isotope thermometry

Zijie Ning[a,b], Laiming Zhang[a,b,*], Katharine W. Huntington[c], Chengshan Wang[a,b], Jingen Dai[a,b], Zhongpeng Han[a,b], Benjamin H. Passey[d], Xinyu Qian[a,b], Jiawei Zhang[a,b]

[a] State Key Laboratory of Biogeology and Environmental Geology, China University of Geosciences, Beijing 100083, China
[b] School of the Earth Science and Resources, China University of Geosciences, Beijing 100083, China
[c] Department of Earth and Space Sciences, University of Washington, WA 98195-1310, United States
[d] Department of Earth and Environmental Sciences, University of Michigan, MI 48109 United States

ARTICLE INFO

Keywords:
Southern Tibet
Liuqu Conglomerate
Burial depth
Clumped isotope thermometry

ABSTRACT

The Liuqu Conglomerate, exposed along the Yarlung Zangbo suture zone (YZSZ) in southern Tibet, archives not only the process of the India-Asia collision, but also the exhumation history of the India-Asia collision zone. The burial and exhumation history of the Liuqu Conglomerate thus could potentially provide clues to the India-Asia collision and orogeny. Low-temperature thermochronometric data indicate that maximum burial temperatures of the Liuqu Conglomerate ranged from 80 to 110 °C; however, the exact burial history is not well constrained. Here, we examine the burial conditions of the Liuqu Conglomerate by applying clumped isotope thermometry to paleosol carbonates. Extensive microcrystalline recrystallization indicates that the samples have been diagenetically altered during burial. Moreover, the clumped isotope temperatures (ranging from ~48 to ~97 °C) are clearly above Earth surface conditions, indicating the original climatic information was overwritten by alteration at higher burial temperatures. Nevertheless, the calculated diagenetic water $\delta^{18}O$ values represent maximum meteoric water values that can be used to broadly constrain the paleoelevation. The highest clumped isotope temperature implies that the maximum burial temperature of the Liuqu Conglomerate was at least ~97 °C. We conclude that the Liuqu Conglomerate was buried as deeply as 3.7–4.3 km during the latest Paleocene to Eocene, and then exhumed during the Miocene (~10–12 Ma). Incision of the paleo-Yarlung River was likely responsible for erosion and exhumation of the Liuqu Conglomerate, which suggests that the drainage system of Paleo-Yarlung River was similar to that of today and supports the model of outward growth of the Tibetan Plateau.

1. Introduction

The Himalayan-Tibetan orogen, formed by the convergence of the India and Asia continents during the Cenozoic, is the highest topographic feature on Earth, and its orogeny process has attracted a lot of attention (e.g. Harrison et al., 1998; Yin and Harrison, 2000; Wang et al., 2014). The Liuqu Conglomerate, the exterior molasse to the south of the east-west-trending Cenozoic Yarlung Zangbo suture zone (YZSZ), is located between the India continent and Lhasa terrane and thus archived the post-collision orogeny process of southern Tibet and Himalaya (Wang et al., 2000; Ding et al., 2005; DeCelles et al., 2011). The burial and exhumation history of the Liuqu Conglomerate, therefore, is closely related to processes during the early-stage collision (e.g. the demise of the Tethys ocean, crustal deformation, and geographic evolution) and may help to clarify the tectonic evolution of the Himalayan-Tibetan Plateau (Wang et al., 2000; Aitchison et al., 2002; Davis et al., 2004).

Previous studies have examined the stratigraphy and thermal history of the Liuqu Conglomerate (Aitchison et al., 2002; Davis et al., 2002, 2004; Wang et al., 2010; Li et al., 2015a; Qian et al., 2015; Ding et al., 2017; Leary et al., 2016, 2017). Regional mapping and stratigraphy of Davis et al. (2002) indicate that the total thickness of the Liuqu Conglomerate was more than 3.5 km, and outcrops of the unit near the town of Liuxiang (Liuqu) expose ~2 km of stratigraphic thickness (Leary et al., 2016). Recently, various low-temperature thermochronological studies have been applied to constrain the thermal history of the Liuqu Conglomerate near the town of Liuxiang (Li et al., 2015a). Apatite (U-Th)/He (AHe) data imply that peak burial temperatures exceeded ~80 °C, while apatite fission track (AFT) data imply

* Corresponding author.
E-mail address: lzhang@cugb.edu.cn (L. Zhang).

https://doi.org/10.1016/j.jseaes.2018.12.009
Received 11 July 2018; Received in revised form 5 December 2018; Accepted 5 December 2018
Available online 15 December 2018
1367-9120/

that the peak burial temperatures were less than ~110 °C, and possibly 90 ± 5 °C based on the ages for the sub-population of apatites with low Cl content (< 0.2 wt%) (Li et al., 2015a). Burial conditions are also thought to have reset oxygen stable isotopic values from the Liuqu Conglomerate deposits (Leary et al., 2017). This paper is framed around understanding the burial history from another perspective, namely studying diagenetic alteration of paleosol carbonates in the basin using clumped isotopes, and synthesizing constraints on basin history and implications for the orogeny.

In this study, we collected paleosol carbonate nodules from the type section of the Liuqu Conglomerate in the Liuqu Basin near Liuxiang town (Wang et al., 2010; Qian et al., 2015) for petrographic study and clumped-isotope thermometry (Δ_{47}) analysis. Clumped isotope thermometry provides temperatures of diagenetic carbonate formation during burial without needing to know the $\delta^{18}O$ of diagenetic fluids (Eiler, 2007, 2011; Huntington et al., 2011; Huntington and Lechler, 2015). These data also may help inform interpretations of previous conventional stable oxygen isotopic data from the Liuqu Conglomerate, which were affected by diagenetic alteration and were of limited use in reconstructing the history of the basin (Leary et al., 2017). Finally, we integrate our Δ_{47} results and previous thermochronological data to we reconstruct the basin's burial and exhumation history and place constraints on the topographic evolution of the Tibetan plateau.

2. Geological background

The E-W-trending YZSZ in southern Tibet is located between the continents of Asia and India, bordered by the Lhasa Terrane (e.g. Xigaze Basin and Gangdese arc) to the north, and the Tethyan Himalayan fold-and-thrust belt (e.g. Tethyan, Higher and Lesser Himalayans) to the south (Yin, 2006). Its major components are Yarlung Zangpo ophiolites (Hébert et al., 2012) and mélange complexes with ophiolitic, serpentinitic, and sedimentary matrix (Cai et al., 2012), that archive the history of geodynamic and erosional processes following intercontinental collision (Carrapa et al., 2014).

The Liuqu Conglomerate is located in a narrow elongate zone to the south of YZSZ ophiolites and discontinuously extends for more than 150 km from Bailang to Lhazte (Wang et al., 2010). The unit is predominantly composed of reddish conglomerates and sandstones deposited in a variety of settings, from alluvial fan and braided river to subaqueous environments (Davis et al., 2002). The conglomerates are generally bedded at a scale of several centimeters up to 4 m and are usually intercalated with reddish silty mudstones and paleosols (Wang et al., 2010). Aitchison et al. (2002) suggested that the Liuqu Conglomerate was deposited directly after the India-Asia collision and thus may archive the uplift history of Himalayan-Tibetan Plateau.

Previous studies suggested that materials derived from the Lhasa and Xigaze terranes are notably absent in the Liuqu Conglomerate (Aitchison et al., 2000; Davis et al., 2002). However, recently, detailed petrographic studies and U-Pb/Hf isotope analyses of detrital zircon indicate that the clasts of the Liuqu Conglomerate were mainly derived from the Xigaze forearc basin to the north of the YZSZ, the Yarlung-Zangbo ophiolite within the YZSZ itself, and the Langjiexue Group and Tethyan Himalayan sedimentary rocks to the south of the YZSZ (Wang et al., 2010; Leary et al., 2016). The presence of materials derived from these units shows that the Liuqu Conglomerate was indeed deposited after the collision between the Indian and Asian continents (e.g. Wang et al., 2010; Leary et al., 2016).

Ages ranging from Paleocene to Miocene have been suggested for the Liuqu Conglomerate (Fig. A1; Wei et al., 2011; Li et al., 2015a; Ding et al., 2017), with paleontological constraints varying considerably. Evidence from plant fossils has been interpreted to indicate that the Liuqu Conglomerate was formed in the Eocene (Tao, 1988; Fang et al., 2006). In contrast, palynologic results suggest that the Liuqu Conglomerate includes Oligocene deposits and may consist of Eocene or Miocene deposits (Wei et al., 2011).

Several lines of evidence, including biotite $^{40}Ar/^{39}Ar$ data, detrital zircon fission-track analyses, and $\delta^{13}C$ compositions of soil carbonates, have been interpreted to suggest that the Liuqu Conglomerate was deposited later, significantly after collision at ca. 20–19 Ma (Li et al., 2015a; Leary et al., 2016). However, these lines of evidence may have multiple interpretations. For example, although the $^{40}Ar/^{39}Ar$ age of a crosscutting dike in the Liuqu Conglomerate is 20 Ma (Leary et al., 2016), this result suggests that the Liuqu Conglomerate was older than 20 Ma rather than indicating that it was deposited at 20 Ma. Thermochronologic data are the key evidence cited in support of a Miocene age, but the dataset is limited dataset (15 and 25 Ma, Leary et al., 2016) and not unambiguous, which allows for other interpretations. $\delta^{13}C$ compositions of soil carbonates support both Miocene and Eocene ages (Fig. A1).

However, two recent zircon U-Pb datasets corroborate each other and confirm the deposit is latest Paleocene/earliest Eocene in age. Detrital zircon U-Pb analysis of the Liuqu Conglomerate provides a latest Paleocene maximum age of 58 ± 1 Ma (Wang et al., 2010). Recent tuffite zircon U-Pb dating reveals an age of ca. 59 Ma (Ding et al., 2017) that is consistent with this detrital zircon maximum age. Together, these two radiometric dating approaches tightly constrain deposition of the Liuqu Conglomerate to ~58–59 Ma.

3. Material and methods

3.1. Sample collection and preparation

Our study was conducted near Liuxiang town, Xigaze (Fig. 1), where the width of the exposed the Liuqu Conglomerate from north to south is greatest, with a thickness of ~1800 m (Fig. 2). In this section, the Liuqu Conglomerate uncomfortably overlies the Yarlung-Zangbo ophiolite in the north and the Mesozoic low-grade metasedimentary rocks of the Tethyan Himalayan sequences in the south (Yin, 2006). Many paleosols were recognized in the Liuqu Conglomerate beneath grey to green conglomerates or coarse sandstone with erosional basal surfaces. In this study, we collected 35 paleosol carbonate nodules from 4 reddish paleosol layers (Fig. 2). These nodules are 1–3 cm in diameter and were located > 50 cm below the paleosol surfaces.

The petrographic characteristics and stable/clumped isotope compositions of ancient carbonates may be diagenetically altered during the burial process (e.g. Huntington et al., 2011; Henkes et al., 2014). For all our samples, standard petrographic thin sections were examined using an Olympus BX51 optical microscope that allowed observations under the natural and polarized light. The samples were also examined under cathodoluminescence (CL) using a Technosyn Luminoscope operated at 12–15 kV, 650–550 mA, and 0.03 torr pressure. To collect sample material for isotopic analysis, carbonate powder from polished surfaces of the samples was obtained using a micro-drill. Large veins were avoided in sampling, and the polished surfaces were drilled no deeper than 2 mm to avoid unintentionally drilling vein carbonate.

3.2. Stable isotope analysis

In this study, 28 of the 35 collected paleosol carbonate nodules were selected for stable oxygen and carbon isotope analysis. The stable isotope analyses were performed with a GV Isoprime II stable isotopic mass spectrometer at China University of Geosciences, Beijing. Prior to the analyses, sample carbonate powder was heated at 150–200 °C in a vacuum for 3–4 h. CO_2 was produced by 100% phosphoric acid digestion of 2 mg of carbonate powder from each sample at 90 °C. In this

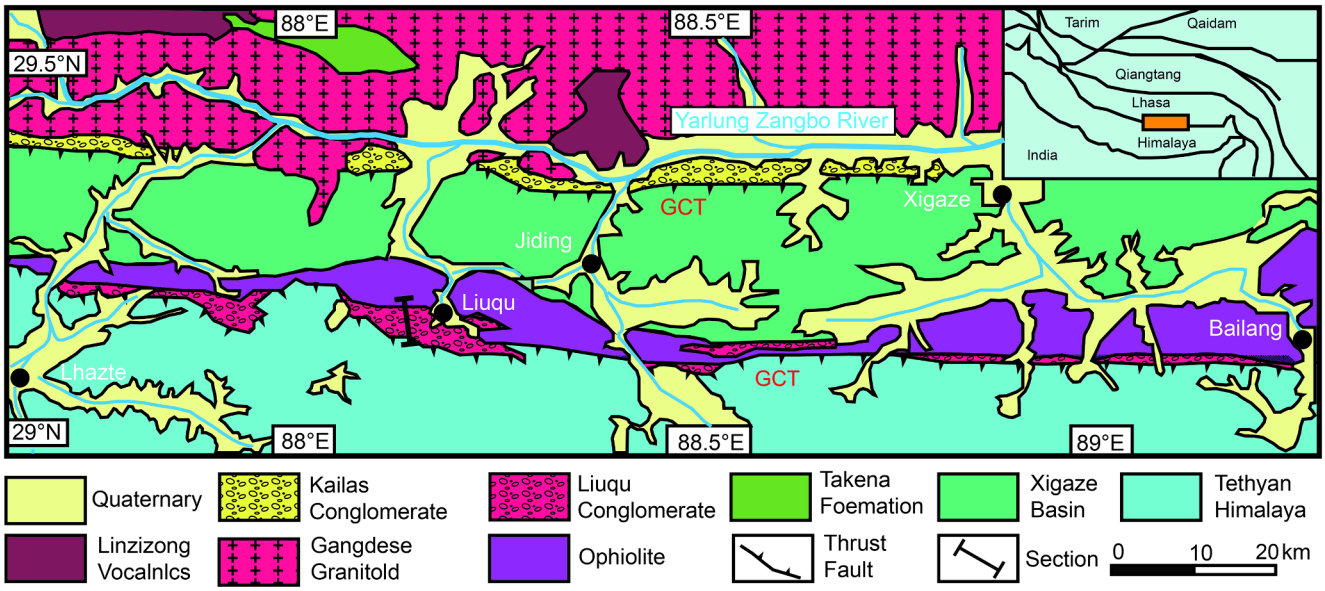

Fig. 1. Simplified geological map of Xigaze region, Southern Tibet, modified after Li et al. (2015a, 2015b). GCT = Great Counter Thrusts; TH = Tethyan Himalaya; K = Kailas; Z = Zedang.

study, the results are corrected relative to the international standards NBS-18 and NBS-19. The carbonate $\delta^{18}O_c$ and $\delta^{13}C_c$ values (denoted with subscript "c") are reported in δ notation (in ‰) relative to VPDB. The standard deviations (σ) of the standards are better than 0.2‰ and 0.15‰ for $\delta^{18}O$ and $\delta^{13}C$, respectively.

3.3. Clumped isotope analysis

Carbonate clumped-isotope (Δ_{47}) thermometry is based on the proportion of molecules containing two heavy isotopes (^{13}C and ^{18}O) in carbonate minerals relative to the random distribution, which is sensitive to the mineral growth temperatures and independent of bulk isotopic composition (Ghosh et al., 2006; Schauble et al., 2006; Eiler, 2007, 2011). The Δ_{47} parameter is a measure of the relative amount of $^{13}C^{18}O^{16}O_2^{2-}$, which decreases with increasing temperature of equilibration (Schauble et al., 2006) and thus records the temperature of primary or diagenetic mineral formation (e.g. Huntington et al., 2011) or the effects of post-depositional reheating (e.g. Passey and Henkes, 2012; Henkes et al., 2014; Stolper and Eiler, 2015; Lloyd et al., 2017). Therefore, clumped isotopes may archive temperatures during the burial processes (Huntington et al., 2011; Passey and Henkes, 2012; Henkes et al., 2014; Shenton et al., 2015) and can constrain the thermal history of sedimentary units (e.g. Shenton et al., 2015; Methner et al., 2016; Gallagher et al., 2017). In addition, the $\delta^{18}O$ of fluid ($\delta^{18}O_w$) from which carbonates formed can be calculated based on the $\delta^{18}O_c$ and clumped isotope temperatures ($T(\Delta_{47})$) to help to constrain the burial history.

We selected 7 carbonate nodules from 3 paleosol layers (upper, middle, lower) to conduct clumped isotope analyses at Johns Hopkins University following the method of Passey et al. (2010). The CO_2 was obtained from 8 mg of pure carbonate powders (or equivalent impure carbonate powders) by reacting with 100% phosphoric acid at 90 °C for 10 min. After being purified, the CO_2 was introduced to a Thermo Scientific MAT 253 mass spectrometer using an automated system. Δ_{47} values were reported relative to the carbon dioxide equilibrium scale, or absolute reference frame (ARF) by periodically analyzing aliquots of enriched/depleted CO_2 that were isotopically equilibrated at 30 °C or 1000 °C (Dennis et al., 2011). One of three internal carbonate standards, HAF Carrara, NBS-19, or 102-GC-AZ01 was analyzed every day alongside samples to monitor system stability and precision.

Δ_{47} calculations were made using the methods of Huntington et al. (2009), except that the ^{17}O correction parameters of Brand et al. (2010) were used based on the recommendations of Daëron et al. (2016) and Schauer et al. (2016), with R13 (VPDB) of 0.011180, R17 (VSMOW) of 0.00038475, and the λ value of 0.528. The Δ_{47} temperatures were calculated using the calibration of Kelson et al. (2017), which is based on synthetic carbonates that were reacted at 90 °C and Δ_{47} values that are reported in the absolute reference frame and calculated with these updated ^{17}O correction parameters. The $\delta^{18}O_w$ of soil water was calculated using the fractionation equation of Kim and O'Neil (1997), and water $\delta^{18}O_w$ values (denoted with subscript "w") are reported relative to VSMOW.

In this study, the heated gas line (1000 °C) and the equilibrium gas line (30 °C) are consistent throughout the entire analyses. The deviation of sample Δ_{48} values from the heated gas Δ_{48} line was < 1‰ in magnitude for all of the samples. The long-term averages are HAF Carrara (n = 5) Δ_{47} = 0.398 ± 0.005‰, NBS-19 (n = 5) Δ_{47} = 0.405 ± 0.011‰, and 102-GC-AZ01 (n = 9) Δ_{47} = 0.695 ± 0.007‰ (ARF, mean ± 1σ standard deviation) for the first session; and HAF Carrara (n = 19) Δ_{47} = 0.392 ± 0.010‰, NBS-19 (n = 21) Δ_{47} = 0.391 ± 0.011‰, and 102-GC-AZ01 (n = 35) Δ_{47} = 0.697 ± 0.012‰ (ARF, mean ± 1σ standard deviation) for the second session.

4. Results

4.1. Petrography

All the samples were examined with polarized light microscopy, and most samples were also examined with CL microscopy (Figs. 3 and A2). The matrices of paleosol carbonates are pervasively recrystallized microspar (Fig. 3) with minor cross-cutting veins filled with sparry calcite (Fig. 3). The samples from the middle and lower layer are full of large spar and sparry veins, with inhomogeneous matrix. The samples from the upper layer show more homogeneous and less sparry veins, while

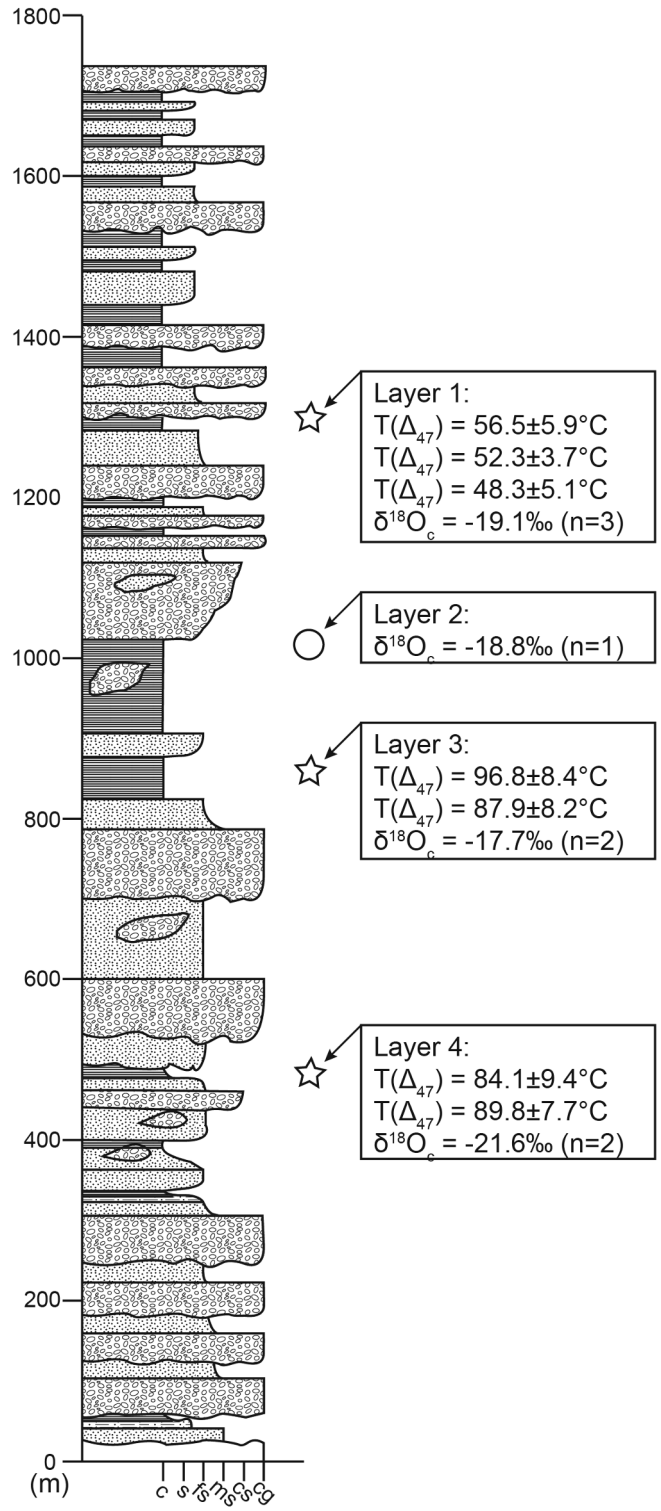

Fig. 2. A generalized stratigraphic column of the Liuqu Conglomerate. The depth of samples, clumped isotope, and average stable isotopic data are also shown. The stars represent the samples with stable and clumped isotopic data. The circle represents the sample with only stable isotopic data.

extensive microspar still could be observed (Figs. 3 and A2). Both the microspar portions and sparry veins generally exhibit similar luminescence in a given sample (i.e., dull red or non-luminescence (Fig. 3), with minor (< 100 μm-scale) bright yellow luminescent zones.

4.2. Bulk isotope ($\delta^{13}C_c$ and $\delta^{18}O_c$) and clumped isotope results

The bulk isotope ($\delta^{13}C$ and $\delta^{18}O$) and clumped isotope results are presented in Table 1 and Fig. 4. The $\delta^{18}O_c$ values range from −24.2 to −16.1‰ with an average value of −19.1‰. The $\delta^{13}C_c$ values range from −12.0 to −6.9‰ with an average value of −9.2‰. Our C and O isotopic results are generally consistent with Liuqu paleosol carbonate values of Leary et al. (2017), but our samples show a broader range extending to more negative $\delta^{18}O_c$ values (Fig. 4).

The Δ_{47} values range from 0.608 to 0.515‰, which yield $T(\Delta_{47})$ values that range from 48 °C to 97 °C (Table 2 and Fig. 2). The clumped isotope temperatures and C and O isotopic values vary by paleosol horizon. The upper layer (layer 1, Fig. 2) temperatures range from 48 °C to 56 °C, with an average value of 52 ± 5 °C (95% confidence; n = 3); the calculated $\delta^{18}O_w$ values range from −13.2 to −10.7‰ VSMOW (Fig. 5). The middle layer (layer 3, Fig. 2) yields higher temperatures of 88 and 97 °C, with an average value of 92 ± 9 °C (95% confidence; n = 2), and higher calculated $\delta^{18}O_w$ values of −5.0 and −3.7‰. The lower layer (layer 4, Fig. 2) yields temperatures of 90 and 84 °C, with an average value of 87 ± 6 °C (95% confidence; n = 2) that is statistically indistinguishable from the middle layer temperature; the lower layer calculated $\delta^{18}O_w$ values of −9.2 and −9.0‰ are lower than the middle layer values.

5. Discussion

5.1. Constraints on diagenetic history from clumped isotope temperatures

Obviously, our $T(\Delta_{47})$ values in excess of ca. 50 °C are too high to represent ancient surface temperature. The paleolatitude of the Liuqu Conglomerate was ~15°N during the Eocene (Liebke et al., 2010; Sun et al., 2012), and previous studies suggested that the Liuqu Conglomerate was deposited at a relatively low elevation (~1 km or lower) in a tropic to subtropic environment (Fang et al., 2006; Ding et al., 2017; Leary et al., 2017). Based on TEX_{86} thermometry, the warmest tropical sea surface temperatures were about 35–40 °C during the Eocene (Huber, 2008). Even taking the low latitude and elevation, and summer bias of soil carbonate formation and solar heating into account (Passey et al., 2010; Quade et al., 2013), our results are much higher than the reasonable Eocene tropical Earth surface conditions. Therefore, we suggest that our Δ_{47} values were altered by burial diagenesis, which is consistent with the petrographic characteristics observed under the microscope and CL (Fig. 3), and previous interpretations of conventional oxygen isotopic results (Leary et al., 2017).

Δ_{47} values may be altered by solid-state reordering of C—O bonds or open/closed-system recrystallization processes during burial diagenesis (Dennis and Schrag, 2010; Passey and Henkes, 2012). Solid-state reordering of C—O bonds in the carbonate mineral lattice is sensitive to the sample temperature-time history (Passey and Henkes, 2012; Henkes et al., 2014; Stolper and Eiler, 2015). Previous experiments indicate that burial/reheating temperatures of ~100 °C or below for timescales of 10^6–10^8 years hardly lead to solid-state C—O bonds reordering (Henkes et al., 2014). Since the C—O bonds break and reform at the molecular scale, this process would change the primary clumped isotope compositions with no change on the texture and stable isotope compositions of the calcite.

It is unlikely that the samples were affected by solid-state reordering of Δ_{47} values due to reheating in the absence of carbonate dissolution and re-precipitation. No magmatism has been reported in this region (Davis et al., 2002; Wang et al., 2010; Leary et al., 2016), so sample reheating was limited to the burial temperature-time history of the sampled units. Apatite (U-Th)/He (AHe) data show complete post-

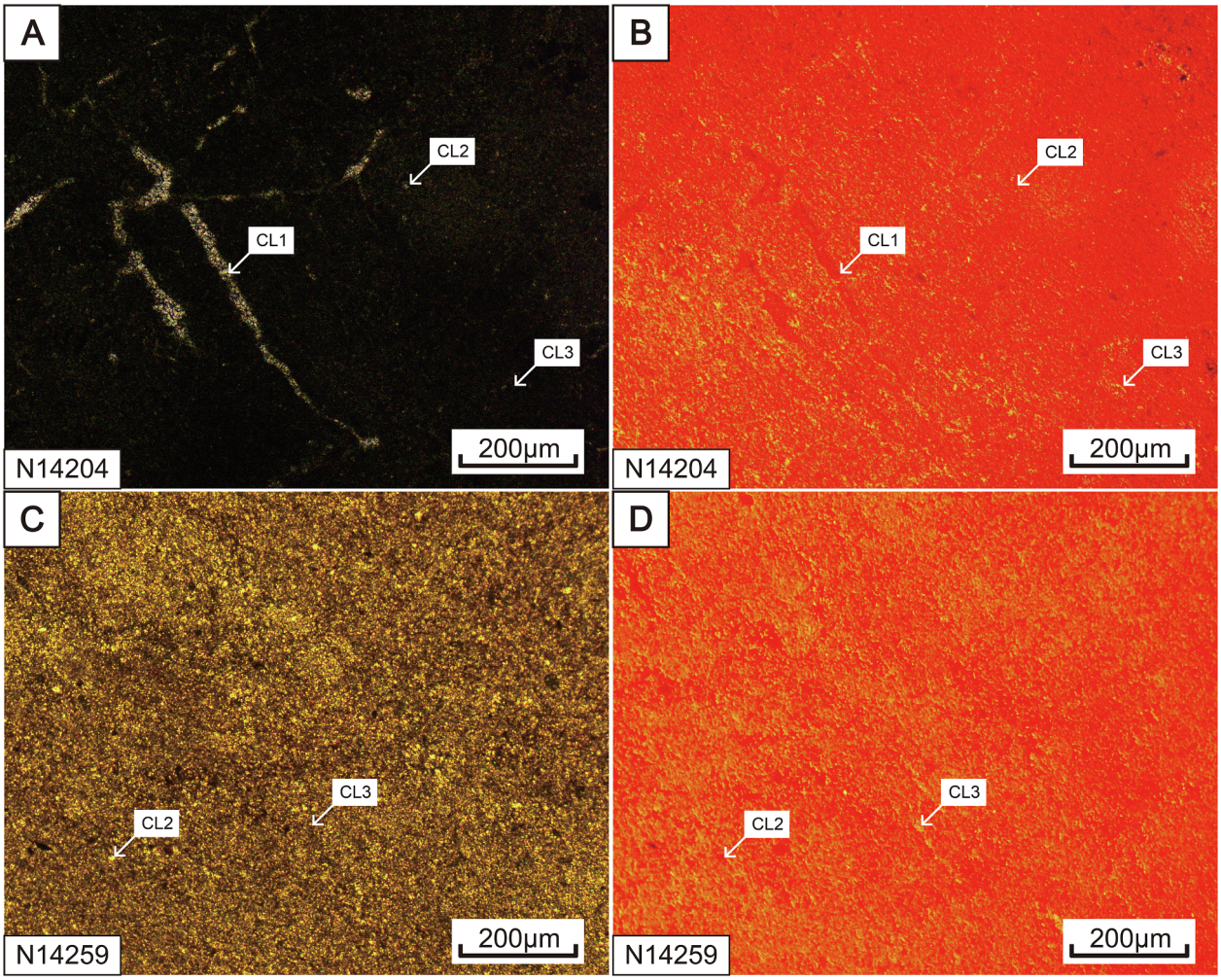

Fig. 3. Paired plane light (A and C) and cathodoluminescent (CL, B and D) photomicrographs of paleosol carbonate nodules. The micrite, microspar and little veins could be observed. The veins are filled with calcite spar (dull red luminescent, CL1). The microspar is dull red luminescent (CL2) and micrite is bright yellow luminescent (CL3). (For interpretation of the references to colour in this figure legend, the reader is referred to the web version of this article.)

depositional thermal resetting of the entire section we sampled, indicating minimum burial temperatures in excess of ~80 °C (Li et al., 2015a). Apatite Fission Track (AFT) data with multi-peak distributions imply incomplete post-depositional thermal resetting with maximum burial temperatures of less than ~110 °C (Li et al., 2015a). Assuming a worst-case scenario of rapid burial to a temperature of 110 °C for a duration of 50 My followed by rapid exhumation and cooling, the model of Passey and Henkes (2012) predicts a change in apparent $T(\Delta_{47})$ due to solid-state reordering of less than 1 °C (Fig. A3). We thus conclude that the observed $T(\Delta_{47})$ values are temperatures of diagenetic calcite growth during burial and most likely reflect the thermal history of the basin under rapid subsidence (Davis et al., 2002; Wang et al., 2010).

This interpretation is consistent with the petrographic and CL observations, which we interpret to indicate pervasive recrystallization of the samples. Differences in luminescence indicate changes of the manganese and ferrum contents of water from which the cement grew (Sears, 1989; Machel and Burton, 1991), so the similarity of spar and microspar luminescence may suggest pervasive recrystallization in the presence of similar diagenetic fluids. Indeed, the tiny veins observed in the samples were caused by fracture of the samples on a microscopic scale, which could have promoted alteration (VanDeVelde et al., 2013). In general, micritic nodules are more common in unaltered soils (Wieder and Yaalon, 1974, 1982); our samples possess a granular texture under transmitted light and appear speckled under CL, which indicate extensive recrystallization of the micritic matrix (VanDeVelde et al., 2013). Therefore, we concluded that our samples were pervasively recrystallized during burial (VanDeVelde et al., 2013; Wieder and Yaalon, 1982; Garzione et al., 2004; Leier et al., 2009).

Clumped isotope temperatures of ~84 to 97 °C for the lower and middle paleosols are similar to the maximum burial temperature constraints given by AHe and AFT thermochronology (Li et al., 2015a, 2015b), suggesting that the recrystallization occurred near maximum burial. Apatite cooling ages constrain the timing of maximum burial to be prior to 10–12 Ma (Li et al., 2015a, 2015b), indicating a minimum age for diagenetic alteration of the lower and middle paleosols. Clumped isotope temperatures of ~48 to 57 °C for the upper paleosols are much cooler than those of the other two layers, although they are only 300 m different in stratigraphic depth. We thus suggest that the samples from upper layer were diagenetic recrystallized at much shallower depths, and therefore during a different time period than the lower layers. It is possible that the large temperature differences was

Table 1
Summary of the stable isotopic data for the Liuqu Conglomerates.

Layer	Height (m)	Sample ID	$\delta^{13}C_c$ (‰)[a]	$\delta^{18}O_c$ (‰)[a]
1	487	N14-240	−9.24	−18.02
1	487	N14-241	−12.02	−17.87
1	487	N14-242	−10.66	−18.16
1	487	N14-250	−10.57	−18.86
1	487	N14-251	−9.37	−18.60
1	487	N14-252	−8.65	−21.14
1	487	N14-253	−9.02	−20.06
1	487	N14-254	−7.96	−21.65
1	487	N14-255	−9.22	−19.30
1	487	N14-257	−9.81	−19.59
1	487	N14-258	−9.64	−19.80
1	487	N14-259	−9.87	−18.83
1	487	N14-260	−6.88	−17.08
2	1121	N14-230	−10.32	−18.71
3	852	N14-200	−7.88	−22.22
3	852	N14-202	−7.90	−23.00
4	1277	N14-203	−8.07	−22.34
4	1277	N14-205	−10.42	−16.30
4	1277	N14-206	−10.13	−16.28
4	1277	N14-207	−9.15	−16.59
4	1277	N14-208	−9.30	−16.77
4	1277	N14-209	−9.32	−16.33
4	1277	N14-210	−7.78	−24.24
4	1277	N14-211	−7.91	−21.59
4	1277	N14-213	−8.15	−22.01
4	1277	N14-214	−9.01	−16.13
4	1277	N14-216	−9.24	−16.41
4	1277	N14-217	−10.06	−17.44

[a] Measured versus Vienna Peedee belemnite (VPDB).

caused by different relative proportions of micrite and microspar. However, the CL textures show that the relative proportions of micrite and microspar are similar in our samples, making it difficult to explain the large temperature difference as being due to mixing of different calcite generations.

5.2. Constraints on diagenetic and meteoric $\delta^{18}O_w$

Because the samples were all pervasively recrystallized and not significantly affected by solid-state reordering, $\delta^{18}O_w$ values calculated from the T(Δ_{47}) and $\delta^{18}O_c$ values place constraints on the diagenetic fluid composition at the time of recrystallization. Previous work suggested that the $\delta^{18}O_c$ values of paleosol carbonate nodules from the Liuqu Conglomerate had been reset in a water buffered diagenetic environment (Leary et al., 2017). Leary et al. (2017) showed that marine carbonates within the Liuqu conglomerate do not preserve primary marine $\delta^{18}O_c$ values, but instead record $\delta^{18}O_c$ values that are similar to paleosol $\delta^{18}O_c$ values in the same unit (Fig. 4); the paleosol $\delta^{18}O_c$ values are very low (−20 to −9‰), which Leary et al. (2017) interpret to represent water-buffered recrystallization from meteoric waters. The paleosol $\delta^{18}O_c$ values from our study overlap with the observations of Leary et al. (2017), with even more negative $\delta^{18}O_c$ values as low as −24‰ (Fig. 4). The $\delta^{18}O_c$ values and clumped isotope temperatures for the samples analyzed here place quantitative constraints on the composition of the diagenetic waters, with calculated $\delta^{18}O_w$ values of −9, −4 to 5 and −13 to 10‰ for the lower, middle and upper paleosols, respectively. If the samples represent water-buffered recrystallization from meteoric waters as proposed by Leary et al. (2017), these $\delta^{18}O_w$ values constrain meteoric water compositions; any fluid-rock interaction would make the reconstructed $\delta^{18}O_w$ values represent maximum meteoric water values.

Maximum meteoric water values can be interpreted broadly in terms of basin paleoelevation. Prior workers have proposed a low elevation (~1 km or lower) depositional environment for the basin based on paleontological and geochemical data (Fang et al., 2006; Ding et al., 2017; Leary et al., 2017). The lowest $\delta^{18}O_w$ estimate of −9‰ for the ca. 90 °C samples representing near maximum burial temperatures is generally consistent with a moderate elevation (on the order of 2 km) catchment precipitation source. We suggest this interpretation is plausible given that the $\delta^{18}O_w$ value of precipitation at sea level near New Delhi of −5.8‰ has not changed significantly since the Eocene (Quade et al., 2011), although we note that the actual meteoric water value at the time of diagenetic cement deposition could be lower (i.e., due to evaporation and/or water-rock interaction), which would indicate a higher-elevation precipitation source. This possibility combined with the large uncertainties inherent in paleoelevation reconstruction from $\delta^{18}O$ values prevents us from further refining this estimate. These samples could have reached the near-maximum diagenetic temperatures they record as early as Eocene time based on the sedimentation history of the basin (Zhu et al., 2013), or as late as 10–12 Ma, immediately prior to the timing of exhumation and cooling based on

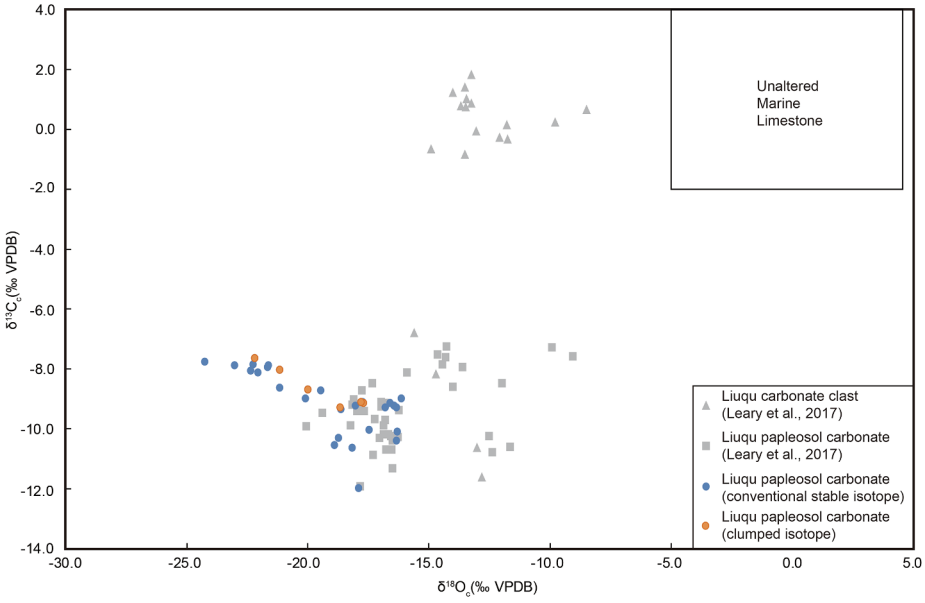

Fig. 4. The plot of oxygen and carbon isotopic results of paleosol carbonate nodules from the Liuqu Conglomerate. Blue and orange circles represent our results from conventional and clumped isotopes. Grey squares and triangles represent data of nodules and clasts from Leary et al. (2017), respectively. The shaded region represents expected isotopic values of marine carbonates (Veizer et al., 1999). VPDB = Vienna Peedee Belemnite. (For interpretation of the references to colour in this figure legend, the reader is referred to the web version of this article.)

Table 2
Summary of the clumped isotopic data for the Liuqu Conglomerates.

Sample ID	Layer	Height (m)	Age	N[a]	$\delta^{13}C_c$ (‰)[b]	$\delta^{18}O_c$ (‰)[b]	Δ_{47} (ARF, ‰)[c]	± 1SE (‰)[d]	T(Δ_{47}) (°C)[e]	± 1SE (°C)	$\delta^{18}O_w$ (‰)[f]	± 1SE (‰)
N14-255	1	487	Eocene	2	−9.118	−17.784	0.624	0.009	48	4	−13.3	0.9
N14-256	1	487	Eocene	2	−8.718	−19.957	0.615	0.018	52	8	−11.3	0.6
N14-259	1	487	Eocene	2	−9.309	−18.654	0.605	0.017	57	8	−10.7	1.0
N14-220	3	852	Eocene	1	−9.166	−17.664	0.526	0.013	97	9	−3.7	1.1
N14-221	3	852	Eocene	1	−9.118	−17.784	0.541	0.013	88	9	−5.0	1.1
N14-204	4	1277	Eocene	1	−8.055	−21.120	0.548	0.013	84	8	−8.9	1.3
N14-212	4	1277	Eocene	1	−7.654	−22.154	0.538	0.013	90	9	−9.2	1.0

[a] Number of unique analysis of CO_2 from carbonate.
[b] Uncertainties on $\delta^{13}C$ and $\delta^{18}O$ are < 0.07 and 0.06% respectively. Measured versus Vienna Peedee belemnite (VPDB).
[c] ARF = Absolute Reference Frame. Acid correction factor is 0.082.
[d] SE = SD/SQRT (N). If the calculated value is smaller than the known precision of the analysis (based on hundreds of repeat measurements of internal standards), were place it with the 'generic' laboratory SE (0.013 for N = 1, 0.009 for N = 2); otherwise we report the larger sample-specific SE. SE = Standard error. SD = Standard deviation.
[e] Calculated using the Eq. (1) in Kelson et al. (2017).
[f] Calculated using the equation for calcite reported in Kim and O'Neil (1997). Measured versus Vienna standard mean ocean water (VSMOW).

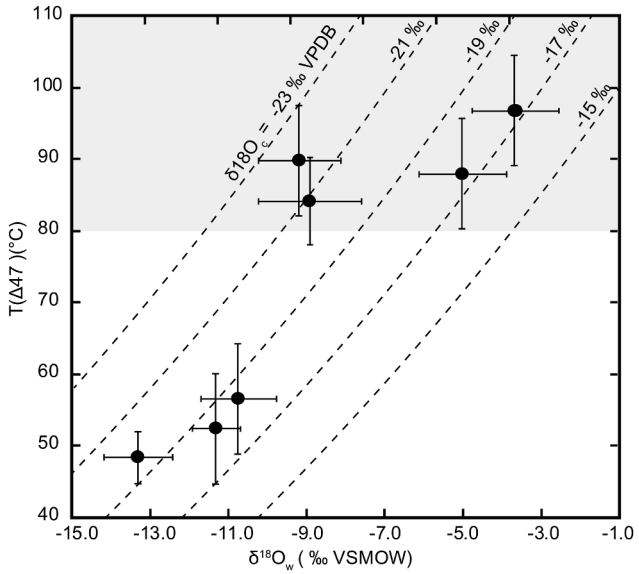

Fig. 5. The T(Δ_{47}) vs. $\delta^{18}O_w$ for paleosol carbonate nodules from the Liuqu Conglomerate. The T(Δ_{47}) were calculated by calibration from Kelson et al. (2017), and $\delta^{18}O_w$ values were calculated by equation from Kim and O'Neil (1997). The errors are showed as black bars (1 SE). The contours of the $\delta^{18}O_c$ were calculated by equation from Kim and O'Neil (1997). The shaded region represents temperature range estimated from low-T thermochronological data (Li et al., 2015a, 2015b). VSMOW = Vienna standard mean ocean water, VPDB = Vienna Peedee Belemnite.

thermochronologic constraints (Li et al., 2015a, 2015b).

The colder clumped isotope temperatures of the upper paleosol suggests that part of the section was altered at a different time in the basin temperature-time history, significantly before or after maximum burial temperature. The lack of cross-cutting relationships and absolute dating of the diagenetic calcites prevent us from ruling out the possibility that the diagenetic fluid circulation in the upper paleosol occurred prior to maximum burial, but we conservatively take the upper paleosol alteration in the presence of isotopically lighter waters to have occurred during exhumation and cooling to ~50 °C later in the basin history. It is difficult to say whether lower $\delta^{18}O_w$ reconstructed for the upper paleosol indicates a change in meteoric water composition and therefore elevation since deposition of the lower and middle paleosols because of the non-primary nature of the samples. Nevertheless, the minimum upper paleosol $\delta^{18}O_w$ value of −13‰ represents a maximum estimate of meteoric water composition, which a simple Raleigh distillation model (Rowley, 2001) suggests is consistent with a minimum elevation for the contributing catchment on the order of 3 km by ~10 Ma.

5.3. Implications for the evolution and exhumation of the Liuqu Conglomerate

Various depositional models have been proposed for the Liuqu Conglomerate (Davis et al., 2002; Wang et al., 2010; Li et al., 2015a). Some researchers suggest that it relates to the collision of the Tethyan intraoceanic island arc with the Indian continent during the Paleogene, predating the final collision between India and Asia continents (Aitchison et al., 2000; Davis et al., 2002; Aitchison et al., 2007). In contrast, others believe that the Liuqu Conglomerate represents low elevation molasse deposition following India-Asia collision, suggesting that Liuqu Conglomerate deposition was contemporary with uplift and erosion of the YZSZ due to ongoing crustal thickening (Einsele et al., 1994; Wang et al., 2010; Qian et al., 2015; Ding et al., 2017). Other recent workers have proposed that the Liuqu Conglomerate represents Early Miocene deposition associated with the paleo-Yarlung River (Li et al., 2015a; Leary et al., 2016, 2017), although this interpretation contradicts evidence from paleobotany and tuffite zircon U-Pb dating that place the onset of the Liuqu Conglomerate deposition at 56 Ma (Ding et al., 2017). Here, we build on previous studies to propose a general scenario for the Cenozoic evolution of the India-Asia collision zone.

A synthesis of previous age estimates indicates that the Liuqu Conglomerate was deposited after India-Asian collision and derived mainly from the north (Wang et al., 2010; Qian et al., 2015). The sedimentary sources for the lower part of the Liuqu Conglomerate in Eocene time included collision-related mélange, the Xigaze forearc basin and the Yarlung-Zangbo ophiolite. The southern margin of the Lhasa terrane (Gangdese arc) had achieved a near-present elevation during this period (Ding et al., 2014), consistent with the topographic gradient decreasing southward toward the Xigaze forearc basin and depocenter of the Liuqu Conglomerate (Fig. 7a). The Xigaze forearc basin itself became a highland after India-Asia collision, although the exact paleoelevation is unknown. To the south of the Liuqu Conglomerate, the relatively low elevation of the suture zone and Tethyan

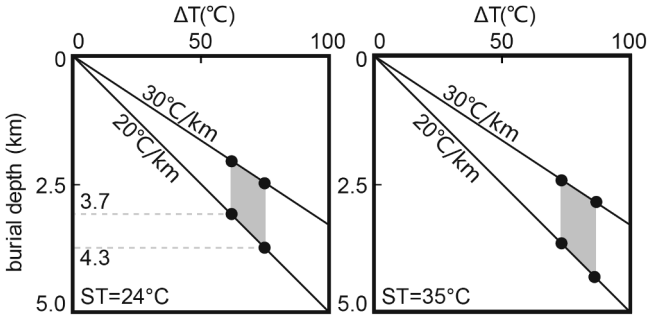

Fig. 6. The plot of temperature difference versus burial depth. The vertical lines represent different burial depth ranges according to different surface paleotemperature during the Eocene and different geothermal gradients. The burial depth between 3.7 and 4.3 km is preferred in this study. ST = surface paleotemperature.

Himalaya led to the development of alluvial fans and braided river systems (Wang et al., 2010; Ding et al., 2017).

The upper part of the Liuqu Conglomerate shows clasts that are mainly derived from the Tethyan Himalaya, indicating that a shift in the sediment source to the south occurred later in the Eocene (Qian et al., 2015). This shift in sedimentary source in the upper part of the conglomerate likely coincided with isostatic uplift of the Tethyan Himalaya induced by Neotethyan slab rollback and breakoff at ~50–45 Ma (Sinclair, 1997; Kohn and Parkinson, 2002; Kellett et al., 2014; Smit et al., 2014; Ji et al., 2016). With slab breakoff, the removal of the load of the subducting slab would have led to the continued uplift of the Tethyan Himalaya. Tethyan Himalayan uplift is also in accordance with the disappearance of the last marine sedimentary rocks in southern Tibet at ~34 Ma (Wang et al., 2002; Jiang et al., 2016). Along with the development of the Eocene-Oligocene Tethyan Himalayan fold belt (Yin, 2006), conglomerates and other deposits were successively deposited in the Liuqu basin and other similar structural depressions along the YZSZ.

Our data and previous observations constrain the burial temperature and maximum stratigraphic thickness of the Liuqu Conglomerate during the Eocene (Fig. 7). Previous thermochronologic data of Li et al. (2015a) suggest peak burial temperatures of ~80 °C (from apatite (U-Th)/He dating) to ~110 °C (from apatite fission track dating). Our maximum clumped isotope temperature refines this estimate, narrowly constraining the peak burial temperature of the Liuqu Conglomerate to between 97 ± 8 °C and ~110 °C. Using this peak burial temperature combined with surface paleotemperature and an assumed paleogeothermal gradient, we estimate a maximum burial depth of 3.7–4.3 km, which is consistent with stratigraphic observations.

Our reasoning supporting this interpretation is as follows. It is likely that the maximum burial depth was attained during the Eocene, based on the latest Paleocene to Eocene depositional age of the bottom of the section (Ding et al., 2017) and lack of deposition after the Eocene (Zhu et al., 2013). At this time, the basin was tropical, near 15° north latitude (Liebke et al., 2010; Sun et al., 2012). Mean annual surface temperature in the relatively low elevation, warm depositional environment of the Liuqu Conglomerate (see Section 5.1) may have been similar to Early Eocene fossil leaf-based estimates of terrestrial equatorial mean annual temperature in the range of ~24 °C (Shukla et al., 2014). The difference between this Eocene Earth surface temperature estimate and the basin maximum depositional temperature of ~97 to 110C (expressed as ΔT) is ~73–86 °C. Assuming a paleogeothermal gradient of 20 °C/km, these ΔT values correspond to maximum burial depth estimates of 3.7 to 4.3 km for the Liuqu Conglomerate (Fig. 6). While only about 2 km of stratigraphic thickness is exposed in the section of the Liuqu Conglomerate sampled here (Leary et al., 2016), regional stratigraphic correlations indicate a total thickness of > 3.5 km (Davis et al., 2002), consistent with this range. Estimates of Latest Paleocene terrestrial equatorial mean annual temperature (~30 °C, based on snake fossil *Titanoboa cerrejonensis*; Head et al., 2009) and Eocene tropical sea surface temperature (35–40 °C, based on a reinterpretation of Tex86 data from Pearson et al., 2007; Huber, 2008) suggest even higher surface paleotemperatures, but a higher surface temperature or higher geothermal gradient result in unreasonably low stratigraphic thickness estimates that are inconsistent with geologic observations (Davis et al., 2002).

Near maximum burial temperature conditions, paleosol carbonates in the lower and middle Liuqu Conglomerate were pervasively recrystallized (Fig. 3) in the presence of deeply circulating meteoric waters in fluid-buffered environment. $\delta^{18}O_w$ values reconstructed from the diagenetic carbonate oxygen and clumped isotope data from these units place maximum constraints on meteoric water oxygen isotopic compositions, which indicate the contributing catchment received precipitation from moderate elevation (minimum elevation of ~2 km). Catchment elevations on the scale of ~2 km at maximum burial are consistent with paleofloral evidence of a low elevation (order 1 km or lower) basin floor earlier in the depositional history of the section (Tao, 1988; Fang et al., 2006; Ding et al., 2017). Carbonates of the Liuqu Conglomerate upper paleosol were recrystallized at temperatures lower than maximum burial conditions, possibly during exhumation and cooling post ~10–12 Ma; reconstructed $\delta^{18}O_w$ values from these diagenetic carbonates are consistent with a minimum elevation of ~3 km for the contributing catchment area, likely in late-Miocene time.

Significant elevation and exhumation of the Liuqu Conglomerate by this time is consistent with constraints on the broad patterns of denudation in the region. The paleo-Yarlung River is thought to have been responsible for denuding a large volume of material from the YZSZ during the Miocene (Carrapa et al., 2014; Li et al., 2015a; Leary et al., 2016). To the north of the Liuqu Conglomerate, the initial exhumation of the Kailas Formation occurred at ~16 Ma (Carrapa et al., 2014; Li et al., 2015a). In the Kailas Formation, ~6 km of strata was denuded by the paleo-Yarlung River (Carrapa et al., 2014) and were then delivered to the Bengal and Indus fans during the Miocene (Decelles et al., 2001; Carrapa et al., 2014; Bernet et al., 2010). To the south of the Kailas Formation, exhumation of the Liuqu Conglomerate commenced slightly later than the Kailas conglomerate, at around 10–12 Ma (Li et al., 2015a) due to the activation of the Great Counter Thrusts (GCT) (Murphy and Harrison, 1999; Yin, 2006; Li et al., 2015b). Our estimate of 3.7 to 4.3 km of depositional thickness of the Liuqu Conglomerate is in accordance with the Davis et al. (2002) estimate of at least 3.5 km of max stratigraphic thickness. Currently, ~2 km of section is still exposed at our field locality, which suggests a maximum sedimentary thickness on the order of 2 km was denuded by the paleo-Yarlung River. Comparing with the 6 km of the Kailas Formation denuded, the exhumation volume of the Liuqu Conglomerate is smaller. The paleo-Yarlung River carried deposits from both Kailas and Liuqu conglomerate along the YZSZ to the Bengal and Indus fans in the Miocene (Hodell et al., 1991; Carrapa et al., 2014; Li et al., 2015a). Not only is the initial exhumation of the Liuqu Conglomerate slightly later than that of the Kailas Conglomerate (Li et al., 2015a), but also the exhumation volume of the Liuqu Conglomerate is smaller than that of the Kailas Conglomerate, which is located on the north side of the YZSZ. This suggests possible southward migration of exhumation accommodated by paleo-Yarlung River incision in the YZSZ area.

We speculate that the drainage area of the paleo-Yarlung River may

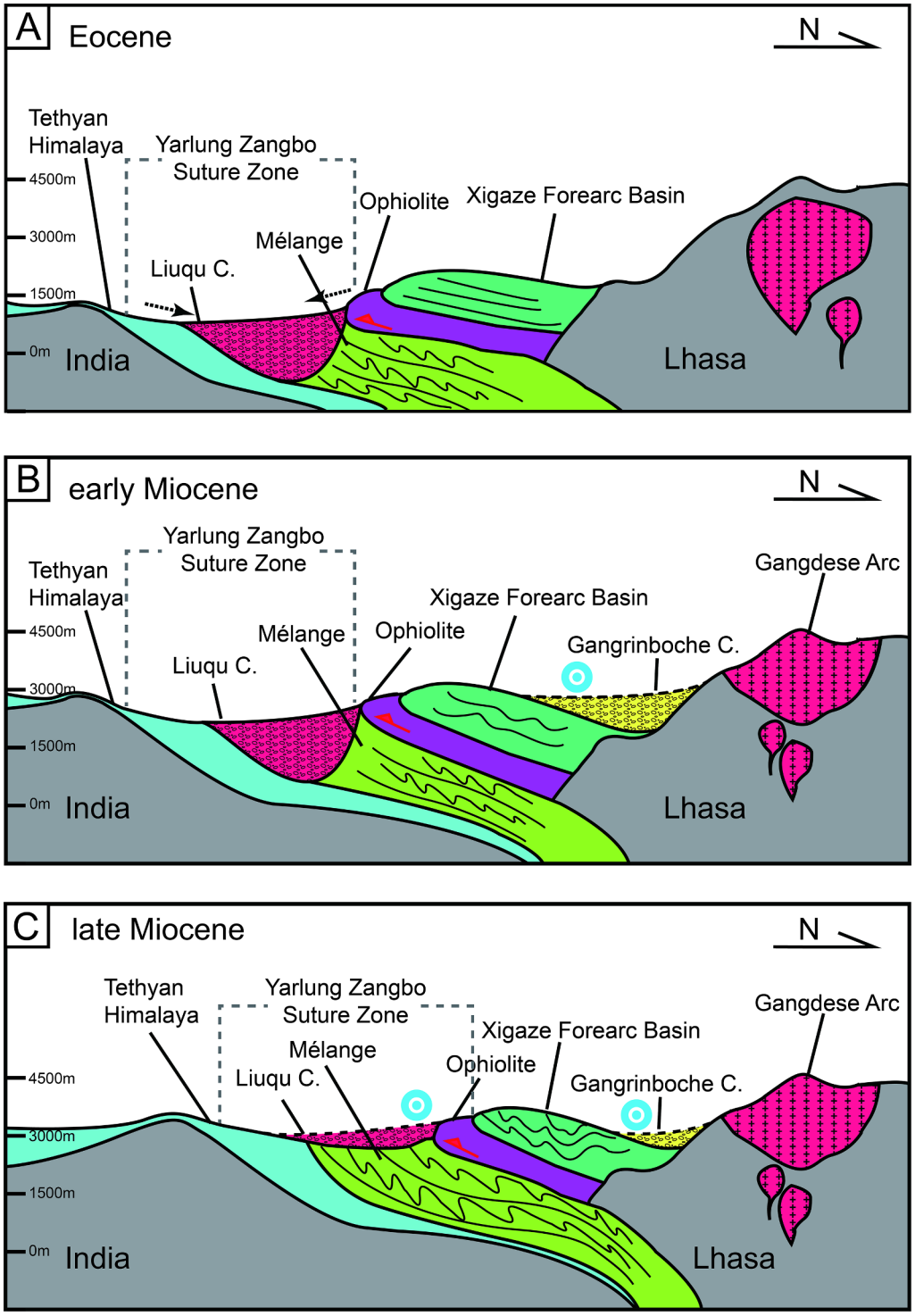

Fig. 7. Tectonic-depositional model for the Liuqu Conglomerate from the Eocene to Miocene. The model is modified after Li et al. (2015a, 2015b). (A) The Liuqu Conglomerate achieved its maximum burial depth of 3.7–4.3 km during Eocene. The dotted arrows suggest the direction of provenance of the Liuqu Conglomerate. (B) the Kailas Conglomerate experienced exhumation by the incision of the Paleo-Yarlung River while Liuqu Conglomerate did not during the early Miocene. The dashed line suggests the exhumation of stratum. (C) the Liuqu Conglomerate experienced exhumation by the incision of the ancestral Yarlung Zangbo river during the late Miocene. The concentric circle suggests that the paleo-Yarlung river from east to west. GCT = Great Counter Thrusts, Liuqu C. = Liuqu Conglomerate, Qiuwu-Dazhuka C. = Qiuwu-Dazhuka Conglomerate.

have expanded and migrated southward between ~16–12 Ma. The rapid evacuation of a large volume of deposits from the YZSZ has been attributed to the enhanced runoff of the paleo-Yarlung River, which was probably in response to the intensification of the Asian monsoon during the Late Miocene (Clift et al., 2008). Independent paleoaltimetry estimates and structural analyses suggest that the Lhasa terrane attained its current elevation prior to the Himalaya orogen (Wang et al., 2008, 2014). This evidence for southward migration of exhumation from the north of YZSZ (the Kailas Conglomerate) to the south of YZSZ (the Liuqu Conglomerate) is consistent with other evidence (e.g. Quantitative paleoaltimetry) for outward growth of the Tibetan Plateau (Wang et al., 2014). Taken together, this history suggests that basin formation and exhumation of the Tethyan Himalaya and the Liuqu Conglomerate was related to both tectonic (e.g. fault motion along the GCT) and

climatic (e.g. Asian Monsoon intensification) factors, both ultimately driven by geodynamics and topographic growth of continental collision.

6. Conclusions

We investigated diagenetic alteration of paleosol carbonates using clumped isotopes, with a goal of better understanding the basin burial and exhumation history by combining the clumped isotope data with low temperature thermochronology data. Recrystallization of the paleosol carbonate nodules and clumped isotope temperatures of 48 to 97 °C confirm that the samples were pervasively recrystallized during burial diagenesis. Nodules from the lower and middle layers were recrystallized at or near peak burial conditions, likely in Eocene time, but possibly as late as mid-Miocene time prior to exhumation ~12–10 Ma. Maximum burial depth estimates of 3.7–4.3 km constrained by the clumped isotope data and previous thermochronologic data are consistent with stratigraphic observations indicating maximum Liuqu Conglomerate thickness of > 3.5 km (Davis et al., 2002). Samples from the upper layer recrystallized at lower temperatures and shallower depths, potentially during exhumation of the Liuqu Conglomerate post ~12–10 Ma. None of the samples were heated sufficiently for their clumped isotope values to be significantly affected by solid-state reordering. As a result, the clumped isotope temperatures and $\delta^{18}O_c$ values can be used to calculate the $\delta^{18}O_w$ compositions of the diagenetic fluids from which the carbonates precipitated. Following Leary et al. (2017), we interpret the diagenetic fluids to represent meteoric waters circulating deeply in the basin at the time of water-buffered carbonate alteration; therefore, the reconstructed diagenetic fluid $\delta^{18}O_w$ values constrain the maximum $\delta^{18}O_w$ values of meteoric water from the contributing catchment. The values broadly suggest the basin paleoelevation was about 3 km in the Miocene, which is consistent with paleoelevation estimates for the Himalaya orogen (Ding et al., 2017). With the uplift of this area, the significant removal of material from the Liuqu Conglomerate was mostly caused by the incision of the paleo-Yarlung River during the Miocene, which suggests that the drainage system of Paleo-Yarlung River was similar to that of today and also supports the model of outward growth of the Tibetan Plateau.

Conflict of interest

The authors declared that they have no conflicts of interest to this work.

Acknowledgments

We thank Dr. Aorigele Zhou and Hailong Zhang for field assistance and Sierra Petersen for assistance with clumped isotope data reprocessing. This study was supported by National Key Research and Development Program of China (2017YFC0601405, 2016YFC0600305), Chinese Academy of Sciences (XDA20070303), and China Geological Survey (DD20160027).

Appendix A

See Figs. A1–A3.

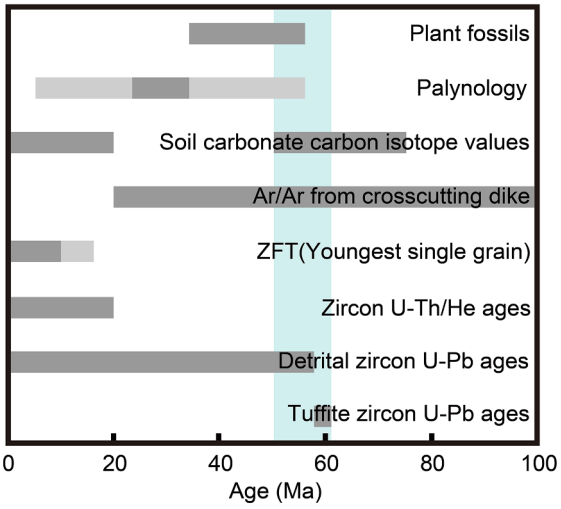

Fig. A1. Compilation of all available geochronologic data for the Liuqu Conglomerate. Dark bars represent the permitted deposition time by each chronometer, with lighter bars showing uncertainty. (modified after Leary et al., 2016). References: plant fossils-Tao (1988) and Fang et al. (2006); palynology-Wei et al. (2011) and Leary et al., 2016; carbon stable isotopes-Ekart et al. (1999); Ar/Ar-Leary et al. (2016); ZFT-Leary et al. (2016); zircon U-Th/He-Li et al. (2015a, 2015b). Derrital zircon U-Pb-Wang et al. (2010) and Ding et al. (2017); Tuffite zircon U-Pb-Ding et al. (2017). ZFT—zircon fission track.

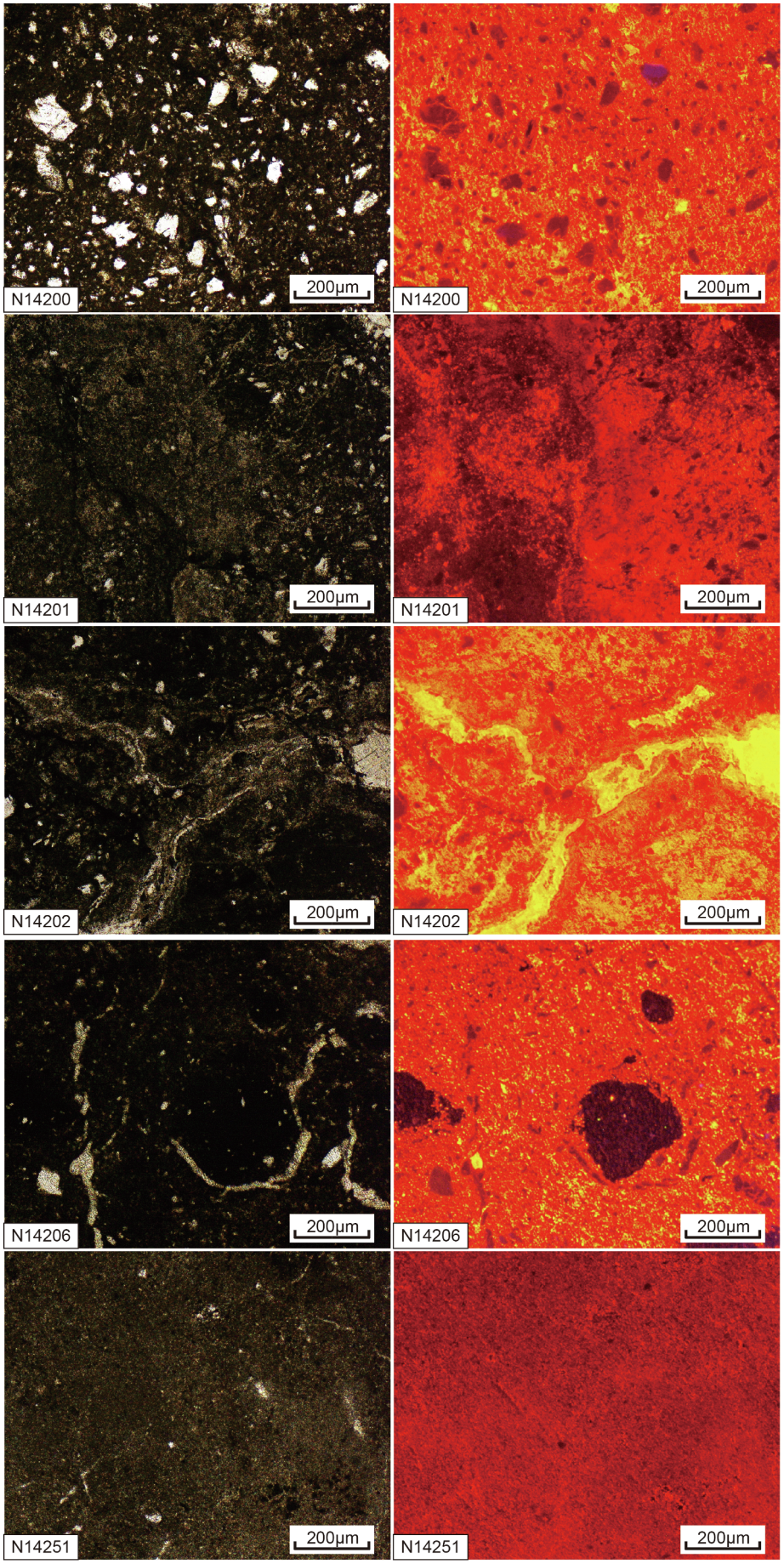

(caption on next page)

Fig. A2. Paired plane light and cathodoluminescent (CL) photomicrographs of some additional paleosol carbonate nodules.

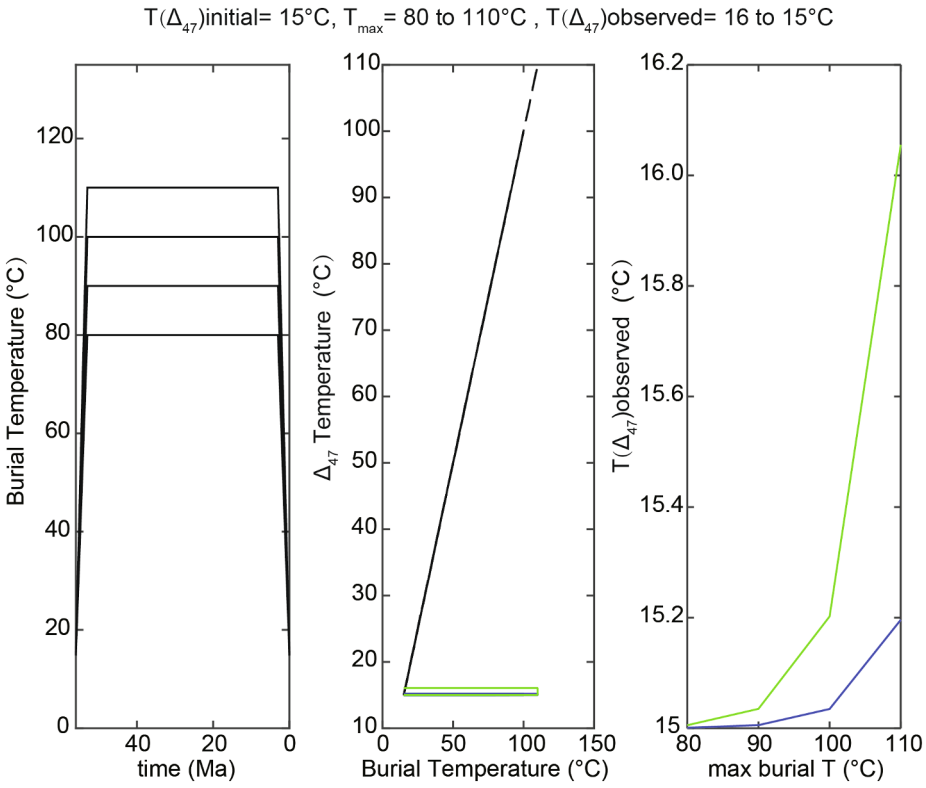

Fig. A3. Modeled temperature-time path following rapid burial to a temperature of 110 °C and rapid exhumation and cooling, as described in text. The model from Passey and Henkes (2012).

Appendix B. Supplementary data

Supplementary data to this article can be found online at https://doi.org/10.1016/j.jseaes.2018.12.009.

References

Aitchison, J., Ali, J., Davis, A., 2007. When and where did India and Asia collide? J. Geophys. Res. B: Solid Earth 112, 1–19.

Aitchison, J.C., Davis, A.M., Liu, J., Luo, H., Malpas, J.G., McDermid, I.R., Wu, H., Ziabrev, S.V., Zhou, M.-F., 2000. Remnants of a Cretaceous intra-oceanic subduction system within the Yarlung-Zangbo suture (southern Tibet). Earth Planet. Sci. Lett. 183, 231–244.

Aitchison, J.C., Davis, A.M., Luo, H., 2002. New constraints on the India-Asia collision: the lower Miocene Gangrinboche conglomerates, Yarlung Tsangpo suture zone, SE Tibet. J. Asian Earth Sci. 21, 251–263.

Brand, W.A., Assonov, S.S., Coplen, T.B., 2010. Correction for the ^{17}O interference in $\delta(^{13}C)$ measurements when analyzing CO_2 with stable isotope mass spectrometry (IUPAC Technical Report): pure and applied chemistry. Pure Appl. Chem. 82, 1719–1733.

Bernet, M., Beek, P.V.D., Pik, R., Huyghe, P., Mugnier, J.L., Labrin, E., Szulc, A., 2010. Miocene to Recent exhumation of the central Himalaya determined from combined detrital zircon fission-track and U/Pb analysis of Siwalik sediments, western Nepal. Basin Res. 18, 393–412.

Cai, F., Ding, L., Leary, R.J., Wang, H., Xu, Q., Zhang, L., Yue, Y., 2012. Tectonostratigraphy and provenance of an accretionary complex within the Yarlung-Zangpo suture zone, southern Tibet: insights into subduction–accretion processes in the Neo-Tethys. Tectonophysics 574, 181–192.

Carrapa, B., Orme, D., DeCelles, P., Kapp, P., Cosca, M., Waldrip, R., 2014. Miocene burial and exhumation of the India-Asia collision zone in southern Tibet: response to slab dynamics and erosion. Geology 42 (5), 443–446.

Clift, P.D., Hodges, K.V., Heslop, D., Hannigan, R., Van Long, H., Calves, G., 2008. Correlation of Himalayan exhumation rates and Asian monsoon intensity. Nat. Geosci. 1, 875–880.

Daëron, M., Blamart, D., Peral, M., Affek, H.P., 2016. Absolute isotopic abundance ratios and the accuracy of Δ47 measurements. Chem. Geol. 442, 83–96.

Davis, A.M., Aitchison, J.C., Hui, L., 2004. Conglomerates record the tectonic evolution of the Yarlung-Tsangpo suture zone in southern Tibet. Geol. Soc. Lond. Spec. Publ. 226, 235–246.

Davis, A.M., Aitchison, J.C., Luo, H., Zyabrev, S., 2002. Paleogene island arc collision-related conglomerates, Yarlung-Tsangpo suture zone, Tibet. Sed. Geol. 150, 247–273.

DeCelles, P., Kapp, P., Quade, J., Gehrels, G., 2011. Oligocene-Miocene Kailas basin, southwestern Tibet: record of postcollisional upper-plate extension in the Indus-Yarlung suture zone. Geol. Soc. Am. Bull. 123, 1337–1362.

Decelles, P.G., Robinson, D.M., Quade, J., Ojha, T.P., Garzione, C.N., Copeland, P., Upreti, B.N., 2001. Stratigraphy, structure, and tectonic evolution of the Himalayan fold-thrust belt in western Nepal. Tectonics 20, 487–509.

Dennis, K.J., Affek, H.P., Passey, B.H., Schrag, D.P., Eiler, J.M., 2011. Defining an absolute reference frame for 'clumped' isotope studies of CO_2. Geochim. Cosmochim. Acta 75, 7117–7131.

Dennis, K.J., Schrag, D.P., 2010. Clumped isotope thermometry of carbonatites as an indicator of diagenetic alteration. Geochim. Cosmochim. Acta 74, 4110–4122.

Ding, L., Kapp, P., Wan, X., 2005. Paleocene-Eocene record of ophiolite obduction and initial India-Asia collision, south central Tibet. Tectonics 24, 1–18.

Ding, L., Spicer, R., Yang, J., Xu, Q., Cai, Q., Li, S., Lai, Q., Wang, H., Spicer, T., Yue, Y., 2017. Quantifying the rise of the Himalaya orogen and implications for the South Asian monsoon. Geology 45, 215–218.

Ding, L., Xu, Q., Yue, Y., Wang, H., Cai, F., Li, S., 2014. The Andean-type Gangdese Mountains: paleoelevation record from the Paleocene-Eocene Linzhou Basin. Earth Planet. Sci. Lett. 392, 250–264.

Eiler, J.M., 2007. "Clumped-isotope" geochemistry—the study of naturally-occurring, multiply-substituted isotopologues. Earth Planet. Sci. Lett. 262, 309–327.

Eiler, J.M., 2011. Paleoclimate reconstruction using carbonate clumped isotope thermometry. Quat. Sci. Rev. 30, 3575–3588.

Einsele, G., Liu, B., Dürr, S., Frisch, W., Liu, G., Luterbacher, H., Ratschbacher, L., Ricken, W., Wendt, J., Wetzel, A., 1994. The Xigaze forearc basin: evolution and facies architecture (Cretaceous, Tibet). Sed. Geol. 90, 1–32.

Ekart, Douglas D., Cerling, Thure E., Montañez, Isabel P., Tabor, Neil J., 1999. A 400 million year carbon isotope record of pedogenic carbonate: implications for paleoatmospheric carbon dioxide. In: American Journal of Science, vol. 299(10), pp. 805–827.

Fang, A., Yan, Z., Pan, Y., Li, J., Yu, L., Liu, X., Huang, F., Tao, J., 2006. The age of the

plan fossil assemblage in the Liuqu Conglomerate of southern Tibet and its tectonic significance*. Prog. Nat. Sci. 16, 55–64.
Gallagher, T.M., Sheldon, N.D., Mauk, J.L., Petersen, S.V., Gueneli, N., Brocks, J.J., 2017. Constraining the thermal history of the North American Midcontinent Rift System using carbonate clumped isotopes and organic thermal maturity indices. Precambr. Res. 294, 53–66.
Garzione, C.N., Dettman, D.L., Horton, B.K., 2004. Carbonate oxygen isotope paleoaltimetry: evaluating the effect of diagenesis on paleoelevation estimates for the Tibetan plateau. Palaeogeogr. Palaeoclimatol. Palaeoecol. 212, 119–140.
Ghosh, P., Adkins, J., Affek, H., Balta, B., Guo, W., Schauble, E.A., Schrag, D., Eiler, J.M., 2006. ^{13}C–^{18}O bonds in carbonate minerals: a new kind of paleothermometer. Geochim. Cosmochim. Acta 70, 1439–1456.
Harrison, T.M., Yin, A., Ryerson, F.J., 1998. Orographic evolution of the Himalaya and Tibetan plateau. Oxford Monogr. Geol. Geophys. 39, 39–72.
Head, J.J., Bloch, J.I., Hastings, A.K., Bourque, J.R., Cadena, E.A., Herrera, F.A., Polly, P.D., Jaramillo, C.A., 2009. Giant boid snake from the Palaeocene neotropics reveals hotter past equatorial temperatures. Nature 457, 715–717.
Hébert, R., Bezard, R., Guilmette, C., Dostal, J., Wang, C., Liu, Z., 2012. The Indus-Yarlung Zangbo ophiolites from Nanga Parbat to Namche Barwa syntaxes, southern Tibet: first synthesis of petrology, geochemistry, and geochronology with incidences on geodynamic reconstructions of Neo-Tethys. Gondwana Res. 22, 377–397.
Henkes, G.A., Passey, B.H., Grossman, E.L., Shenton, B.J., Pérez-Huerta, A., Yancey, T.E., 2014. Temperature limits for preservation of primary calcite clumped isotope paleotemperatures. Geochim. Cosmochim. Acta 139, 362–382.
Hodell, D.A., Mueller, P.A., Garrido, J.R., 1991. Variations in the strontium isotopic composition of seawater during the Neogene. Geology 19, 24–27.
Huber, M., 2008. A hotter greenhouse? Science 321, 353–354.
Huntington, K.W., Eiler, J.M., Affek, H.P., Guo, W., Bonifacie, M., Yeung, L.Y., Thiagarajan, N., Passey, B., Tripati, A., Daëron, M., Came, R., 2009. Methods and limitations of 'clumped' CO_2 isotope (Δ47) analysis by gas-source isotope ratio mass spectrometry. J. Mass Spectrom. 44, 1318–1329.
Huntington, K.W., Budd, D.A., Wernicke, B.P., Eiler, J.M., 2011. Use of clumped-isotope thermometry to constrain the crystallization temperature of diagenetic calcite. J. Sediment. Res. 81, 656–669.
Huntington, K.W., Lechler, A.R., 2015. Carbonate clumped isotope thermometry in continental tectonics. Tectonophysics 647, 1–20.
Ji, W., Wu, F., Chung, S., Wang, X., Liu, C., Li, Q., Liu, Z., Liu, X., Wang, J., 2016. Eocene Neo-Tethyan slab breakoff constrained by 45 Ma oceanic island basalt–type magmatism in southern Tibet. Geology 44, 283–286.
Jiang, T., Aitchison, J.C., Wan, X., 2016. The youngest marine deposits preserved in southern Tibet and disappearance of the Tethyan Ocean. Gondwana Res. 32, 64–75.
Kellett, D.A., Cottle, J.M., Smit, M., 2014. Eocene deep crust at Ama Drime, Tibet: early evolution of the Himalayan orogen. Lithosphere 6, 220–229.
Kelson, J.R., Huntington, K.W., Schauer, A.J., Saenger, C., Lechler, A.R., 2017. Toward a universal carbonate clumped isotope calibration: diverse synthesis and preparatory methods suggest a single temperature relationship. Geochim. Cosmochim. Acta 197, 104–131.
Kim, S.-T., O'Neil, J.R., 1997. Equilibrium and nonequilibrium oxygen isotope effects in synthetic carbonates. Geochim. Cosmochim. Acta 61, 3461–3475.
Kohn, M.J., Parkinson, C.D., 2002. Petrologic case for Eocene slab breakoff during the Indo-Asian collision. Geology 30, 591–594.
Leary, R.J., DeCelles, P.G., Quade, J., Gehrels, G.E., Waanders, G., 2016. The Liuqu Conglomerate, southern Tibet: early Miocene basin development related to deformation within the Great Counter Thrust system. Lithosphere 8, 427–450.
Leary, R.J., Quade, J., DeCelles, P.G., Reynolds, A., 2017. Evidence from paleosols for low to moderate elevation of the India-Asia suture zone during mid-Cenozoic time. Geology 45, 399–402.
Leier, A., Quade, J., DeCelles, P., Kapp, P., 2009. Stable isotopic results from paleosol carbonate in South Asia: paleoenvironmental reconstructions and selective alteration. Earth Planet. Sci. Lett. 279, 242–254.
Li, G., Kohn, B., Sandiford, M., Xu, Z., Wei, L., 2015a. Constraining the age of Liuqu Conglomerate, southern Tibet: implications for evolution of the India-Asia collision zone. Earth Planet. Sci. Lett. 426, 259–266.
Li, Y., Wang, C., Dai, J., Xu, G., Hou, Y., Li, X., 2015b. Propagation of the deformation and growth of the Tibetan-Himalayan orogen: a review. Earth-Sci. Rev. 143, 36–61.
Liebke, U., Appel, E., Ding, L., Neumann, U., Antolin, B., Xu, Q., 2010. Position of the Lhasa terrane prior to India-Asia collision derived from palaeomagnetic inclinations of 53 Ma old dykes of the Linzhou Basin: constraints on the age of collision and post-collisional shortening within the Tibetan Plateau. Geophys. J. Int. 182, 1199–1215.
Lloyd, M.K., Eiler, J.M., Nabelek, P.I., 2017. Clumped isotope thermometry of calcite and dolomite in a contact metamorphic environment. Geochim. Cosmochim. Acta 197, 323–344.
Machel, H.G., Burton, E.A., 1991. Factors governing cathodoluminescence in calcite and dolomite, and their implications for studies of carbonate diagenesis. Soc. Sediment. Geol. Short Course 25, 37–57.
Methner, K., Fiebig, J., Wacker, U., Umhoefer, P., Chamberlain, C.P., Mulch, A., 2016. Eocene-Oligocene proto-Cascades topography revealed by clumped (Δ_{47}) and oxygen isotope ($\delta^{18}O$) geochemistry (Chumstick Basin, WA, USA). Tectonics 35, 546–564.
Murphy, M.A., Harrison, T.M., 1999. Relationship between leucogranites and the Qomolangma detachment in the Rongbuk Valley, south Tibet. Geology 27, 831–834.
Passey, B.H., Henkes, G.A., 2012. Carbonate clumped isotope bond reordering and geospeedometry. Earth Planet. Sci. Lett. 351–352, 223–236.
Passey, B.H., Levin, N.E., Cerling, T.E., Brown, F.H., Eiler, J.M., 2010. High-temperature environments of human evolution in East Africa based on bond ordering in paleosol carbonates. Proc. Natl. Acad. Sci. 107, 11245–11249.
Pearson, P.N., van Dongen, B.E., Nicholas, C.J., Pancost, R.D., Schouten, S., Singano, J.M., Wade, B.S., 2007. Stable warm tropical climate through the Eocene Epoch. Geology 35, 211–214.
Qian, X., Dai, J., Wang, C., Li, Y., Ge, Y., Zhang, J., 2015. Sedimentary environment and provenance of the Liuqu conglomerate, southern Tibet: new constraints on the Paleogene uplift of Yarlung-Tsangpo suture zone. Acta Petrol. Sin. 31, 1313–1326.
Quade, J., Breecker, D.O., Daeron, M., Eiler, J., 2011. The paleoaltimetry of Tibet: an isotopic perspective. Am. J. Sci. 311, 77–115.
Quade, J., Eiler, J., Daëron, M., Achyuthan, H., 2013. The clumped isotope geothermometer in soil and paleosol carbonate. Geochim. Cosmochim. Acta 105, 92–107.
Schauble, E.A., Ghosh, P., Eiler, J.M., 2006. Preferential formation of ^{13}C–^{18}O bonds in carbonate minerals, estimated using first-principles lattice dynamics. Geochim. Cosmochim. Acta 70, 2510–2529.
Schauer, A.J., Kelson, J., Saenger, C., Huntington, K.W., 2016. Choice of ^{17}O correction affects clumped isotope (Δ47) values of CO_2 measured with mass spectrometry. Rapid Commun. Mass Spectrom. 30, 2607–2616.
Sears, D.W., 1989. Cathodoluminescence of Geological Materials. Unwin Hyman, Pergamon, pp. 146.
Shenton, B.J., Grossman, E.L., Passey, B.H., Henkes, G.A., Becker, T.P., Laya, J.C., Perez-Huerta, A., Becker, S.P., Lawson, M., 2015. Clumped isotope thermometry in deeply buried sedimentary carbonates: the effects of bond reordering and recrystallization. Geol. Soc. Am. Bull. 127, 1036–1051.
Shukla, A., Mehrotra, R.C., Spicer, R.A., Spicer, T.E.V., Kumar, M., 2014. Cool equatorial terrestrial temperatures and the South Asian monsoon in the Early Eocene: evidence from the Gurha Mine, Rajasthan, India. Palaeogeogr. Palaeoclimatol. Palaeoecol. 412, 187–198.
Sinclair, H., 1997. Flysch to molasse transition in peripheral foreland basins: the role of the passive margin versus slab breakoff. Geology 25, 1123–1126.
Smit, M.A., Hacker, B.R., Lee, J., 2014. Tibetan garnet records early Eocene initiation of thickening in the Himalaya. Geology 42, 591–594.
Stolper, D.A., Eiler, J.M., 2015. The kinetics of solid-state isotope-exchange reactions for clumped isotopes: a study of inorganic calcites and apatites from natural and experimental samples. Am. J. Sci. 315, 363–411.
Sun, Z., Pei, J., Li, H., Xu, W., Jiang, W., Zhu, Z., Wang, X., Yang, Z., 2012. Palaeomagnetism of late Cretaceous sediments from southern Tibet: evidence for the consistent palaeolatitudes of the southern margin of Eurasia prior to the collision with India. Gondwana Res. 21, 53–63.
Tao, J., 1988. The Paleogene flora and palaeoclimate of Liuqu Formation in Xizang. The Paleoenvironment of East Asia from the Mid-Tertiary. Occasional Pap. Monogr. Centre Asian Stud. 77, 520–522.
VanDeVelde, J.H., Bowen, G.J., Passey, B.H., Bowen, B.B., 2013. Climatic and diagenetic signals in the stable isotope geochemistry of dolomitic paleosols spanning the Paleocene-Eocene boundary. Geochim. Cosmochim. Acta.
Veizer, J., Ala, D., Azmy, K., Bruckschen, P., Buhl, D., Bruhn, F., Carden, G.A., Diener, A., Ebneth, S., Godderis, Y., 1999. $^{87}Sr/^{86}Sr$, $\delta^{13}C$ and $\delta^{18}O$ evolution of Phanerozoic seawater. Chem. Geol. 161, 59–88.
Wang, C., Dai, J., Zhao, X., Li, Y., Graham, S.A., He, D.F., Ran, B., Meng, J., 2014. Outward-growth of the Tibetan Plateau during the Cenozoic: a review. Tectonophysics 621, 1–43.
Wang, C., Li, X., Hu, X., Jansa, L., 2002. Latest marine horizon north of Qomolangma (Mt Everest): implications for closure of Tethys seaway and collision tectonics. Terra Nova 14, 114–120.
Wang, C., Liu, Z., Hébert, R., 2000. The Yarlung-Zangbo paleo-ophiolite, southern Tibet: implications for the dynamic evolution of the Yarlung-Zangbo Suture Zone. J. Asian Earth Sci. 18, 651–661.
Wang, J., Hu, X., Wu, F., Jansa, L., 2010. Provenance of the Liuqu Conglomerate in southern Tibet: a Paleogene erosional record of the Himalayan-Tibetan orogen. Sed. Geol. 231, 74–84.
Wei, L., Liu, X., Yan, F., Mai, X., Li, G., Liu, X., Zhou, X., 2011. Palynological evidence sheds new light on the age of the Liuqu Conglomerates in Tibet and its geological significance. Sci. China Earth Sci. 54, 901–911.
Wieder, M., Yaalon, D.H., 1974. Effect of matrix composition on carbonate nodule crystallization. Geoderma 11, 95–121.
Wieder, M., Yaalon, D.H., 1982. Micromorphological fabrics and developmental stages of carbonate nodular forms related to soil characteristics. Geoderma 28, 203–220.
Yin, A., 2006. Cenozoic tectonic evolution of the Himalayan orogen as constrained by along-strike variation of structural geometry, exhumation history, and foreland sedimentation. Earth Sci. Rev. 76, 1–131.
Yin, A., Harrison, T.M., 2000. Geologic evolution of the Himalayan-Tibetan orogen. Ann. Rev. Earth Planet. Sci. 28, 211–280.
Zhu, J., Liu, Z., Zhang, H., Tian, W., Li, X., Tan, M., Li, Z., Gong, Z., 2013. The Peoples Republic of China Regional Geological Report of Lazi Map (H45C003003) (Scale: 1: 250000). China University of Geosciences Press Co., LTD, Wuhan, pp. 224 (in Chinese).